ORNL/TM-2022/2411

Development and Standup Testing of a System to Observe Fission Gas Release During Transient Heating of Nuclear Fuel Element Segment

Peter Doyle
Jason Harp
Ben Garrison
Kory Linton

April 2022

OAK RIDGE National Laboratory

ORNL IS MANAGED BY UT-BATTELLE LLC FOR THE US DEPARTMENT OF ENERGY

ORNL/TM-2022/2411

Nuclear Energy and Fuel Cycle Division

DEVELOPMENT AND STANDUP TESTING OF A SYSTEM TO OBSERVE FISSION GAS RELEASE DURING TRANSIENT HEATING OF NUCLEAR FUEL ELEMENT SEGMENTS

Peter Doyle
Jason Harp
Ben Garrison
Kory Linton

April 2022

Prepared by
OAK RIDGE NATIONAL LABORATORY
Oak Ridge, TN 37831
managed by
UT-BATTELLE LLC
for the
US DEPARTMENT OF ENERGY
under contract DE-AC05-00OR22725

CONTENTS

LIST OF FIGURES

LIST OF TABLES

ABSTRACT

As part of an effort to increase the burnup of nuclear fuels used in Light Water Reactors, the mechanisms and timing of fission gas release during high temperature transients must be studied. In this work, a system was built to observe fission gas release of fuel element sections under evacuated conditions, at temperatures up to 800 ℃. System capabilities and limitations are overviewed in this report. The system was further tested with a hydrogen-infused titanium foils and gas release was observed in agreement with literature observations. Pressure was monitored with two sensors, and temperature was monitored using a thermocouple and a pyrometer with continuous visual imaging.

1. INTRODUCTION

To increase burnup of nuclear fuel in Light Water Reactors (LWRs), the kinetics of fission gas release under high temperature transients must be understood. Several groups have performed experiments to understand different portions of fission gas release [1–3] and others have conducted work to model gas release, with a particular focus on gas bubble physics [4,5]. Although many important details regarding mechanisms of gas release have been determined by these efforts [6], several outstanding questions remain to be addressed to aid in modeling fission gas behavior under high-burnup conditions. Additionally, transient fission gas release was identified as a critical gap in data available to support the extension of the burnup limit for commercial light water reactors [7]. A key aspect in addressing these questions is development of experiments in which several types of information are gathered simultaneously. The objective of this work was to develop a rapid transient testing technique allowing visual observation of a fuel sample during heating while measuring the amount of fission gas released and collecting fission gas for post-test characterization. Specific capabilities targeted and achieved in this work are listed in Table 2.

Table 1. Targeted capability overview of the Fuel Visualization System

Capability	Target
Sample size	≤ 5 mm^3
High resolution pressure range	≤ 1325 Pa
Maximum measurable pressure	101 kPa
Temperature ramp rate	≤ 50 ℃/min
Maximum sample temperature	800 ℃
Programmable thermal history	Unlimited setpoint and ramp rate combinations
Vacuum atmosphere	Low vacuum achievable with balance inert (He) environment
Radioactive gas collection	Cold trapping of gases and gamma counting
Sample visualization	Optical imaging throughout the test at 3 Hz or better
Sample temperature determination	Thermocouple on sample holder, spectrometer used as a pyrometer to determine sample temperature
Chamber volume	<600 cm^3

2. SYSTEM DESCRIPTION AND STANDUP TEST DESIGN

2.1 SYSTEM DESCRIPTION

To evaluate fission gas release during heating transients, the system was designed to heat a sample while measuring its temperature, visualizing the sample, and monitoring total system pressure. A schematic of the system is shown in Figure 1 in which, a gas inlet stream allows for flow of high purity (99.995%) He to the system as a carrier gas for radioactive gases and for refill during initial evacuations and pressure setting. He is used so that when the radioactive gases are swept into liquid-nitrogen cooled traps (see Figure 1) only the heavier, radioactive gases are captured and the carrier gas can pass through [8]. Gas flow was controlled using a Masterflex EW-32907-51 flow controller with a flow range of 0.01-1 mL/min or a needle valve connected to a Masterflex EW-32907-14 flow meter with a maximum measured flow rate of 1 L/min. Both controllers were obtained from Cole-Parmer, Vernon Hills, Illinois. The flow controller was used to reliably achieve specific pressures and to slowly refill the chamber, whereas the needle valve was used to control gas flow when bringing the chamber to atmospheric pressure and during fission gas sweeping operations. A check valve was used to ensure there was no back-flow of chamber gases into the inlet line. Following the check valve, a Swagelok PTI-S-MC.3-15AQ pressure transducer measured the inlet gas pressure. Finally, an isolation valve was located just prior to the inlet of the heating system. A schematic of the system is shown in Figure 1.

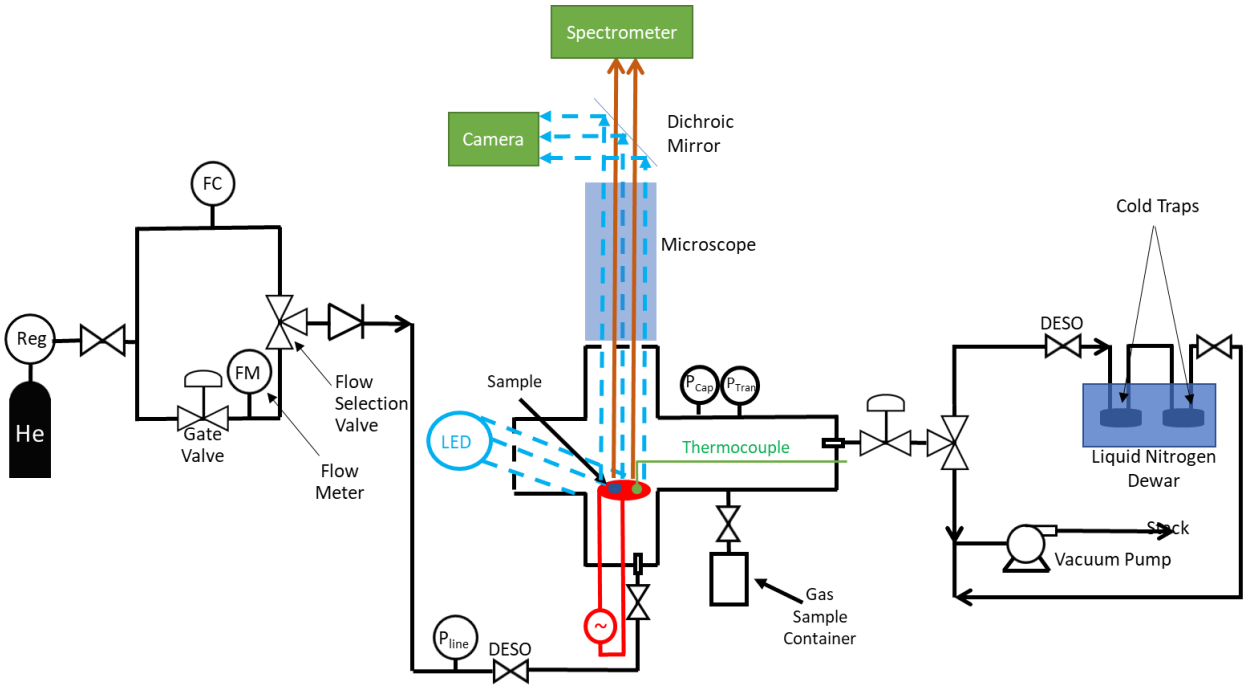

Figure 1. Schematic of the fuel heating and visualization apparatus developed in this work. This schematic shows the major elements of the flow and instrumentation structure. The inlet gas system consists of two gas bottles, isolation valves, two flow controllers, a flow meter, and an inlet line pressure gauge. Inlet gas lines are connected through a double-end shutoff (DESO) valve and can be isolated with the isolation valve directly below the power transfer flange. The heater is shown in red with the sample and heater temperature located on top of the heater where they are illuminated by the light-emitting diode (LED) (blue). A microscope focuses the light, which is separated at the dichroic mirror. Red and infrared light (brown arrows) goes to the spectrometer, and all other light goes to the camera. Two pressure meters (one capacitance meter, and one transducer) are located on the cross. Gas exhausts to the three-way valve to go either through the cold traps or directly to the stack through the vacuum pump.

The heating system consists of a four-way, KF40 cross from Kurt Lesker, Jefferson Hills, Pennsylvania which is equipped with several adapters and instrumentation crosses to monitor the test condition. The gas inlet flange also served as the sample loading location and had a fixed heating element onto which an AlN disk was placed to electrically isolate it from the heating element. AlN disks were cut from an AlN rod sourced from McMaster-Carr, Los Angeles, California (part #6149N13). The heating element is a MC-GAXP-30 spiral 1 in microheater, operated at up to 10 V and 27 A from Micropyretics Heaters International, Cincinnati, Ohio.

The heater power is controlled by a Honeywell UDC3200 proportional–integral–derivative (PID) controller and current limiter from Honeywell Process Solutions, Phoenix, Arizona. The current limiter is connected to the thermocouple (green line in Figure 1) and shuts off power to the heater if the temperature exceeds 1000 ℃. When the circuit is closed, power is controlled by the PID controller, which receives setpoint commands and current temperature readings from the control computer via a LabJack U6-Pro unit from LabJack, Lakewood, Colorado. Temperatures are sent as five volts-of-direct-current (VDC) signals to the PID controller. The LabJack is also used to read the temperature of the type-K thermocouples used for temperature monitoring in this work. In addition to the heater-feedback thermocouple, other thermocouples are used to continuously monitor temperature of potentially hot components on the system. The wires of the thermocouple touching the heater block were insulated using alumina beads to prevent shorting of the signal and avoid the use of polymer-based insulation, which will degrade at the temperatures targeted in this study.

To measure pressure in the system during heating, two pressure meters are located within the vacuum chamber. One is a 902B pressure transducer from MKS Instruments, Longmont, Colorado calibrated for absolute pressure up to 100 kPa. The other is an absolute pressure gauge Kurt Lesker Capacitance Manometer, heated to 45℃ with a pressure range up to 1350 Pa. Both units are separated from the hot zone of the system by several inches of vacuum adapters which are monitored by thermocouples to ensure that temperature limits are not exceeded during the test. The capacitance unit is further installed vertically and is read using a pressure meter controller (VGC501) from Inficon, Balzers, Liechtenstein. Both meters are then read using the appropriate RS232 communication protocol. The 902B and Swagelok transducers are powered using a 1670A power supply from BK Precision, Yorba Linda, California. This supply is also used to power cooling fans that blow lab air onto the heated section of the system to reduce the temperature of the cross.

There are three reasons that both meters are used. Most importantly, the 902B transducer has a much higher range than the capacitance meter and is continuously monitored to ensure that the pressure is kept sub-atmospheric. Because vacuum parts are not rated for positive pressure, when absolute pressure become greater than atmosphere, an explosion hazard exists. As a secondary backstop, a pressure-relief valve is also mounted on the unit (not shown in Figure 1). Secondly, while the transducer does not have the same pressure resolution as the capacitance meter at low pressures, it will provide a secondary verification of pressure recorded by the capacitance meters. In case of instrument errors/failures, significant deviations between the transducer and capacitance meter may occur and allow easier identification. Finally, several evacuations and gas refills are used during the test to flush out air (at the test start) and evolved gases (at the end of the test). For those operations, higher absolute pressures (up to 50 kPa) are used than the capacitance meter can read. The transducer can report those higher refill pressures.

Two viewports are positioned on two arms of the cross. At 90° from the sample port, one viewport is used to convey a collimated LED light into the chamber for indirect lighting of the sample (Thorlabs, Newton, New Jersey, parts M445L4 with SM2F32-A). Directly above the sample, the second viewport is used for imaging and spectroscopy. A K2-Distamax Microscope from Infinity USA, Centennial, Colorado focuses the light on to a Thorlabs DMLP650L dichroic beam splitter, with a splitting wavelength near 650 nm.

Above 700 nm, almost all of the light is transmitted, with shorter wavelengths being reflected. Reflected light from the mirror is captured using a Grasshopper 3 camera, model GS3-U3-41C6C-C, from Teledyne FLIR, Wilsonville, Oregon. Transmitted light was captured with a Thorlabs using a ULS2048XL-EVO spectrometer from Avantes, Louisville, Colorado. The spectrometer is used to infer sample temperature, as described in Section 2.2. Two irises, one just below the microscope and one just below the dichroic mirror are used to optimize sample viewing, while excluding light from non-sample sources. This microscope system was mounted on an XY translation stage to allow selection of viewing location.

Finally, system volume is determined using a gas sample cylinder of known volume (Swagelok 25 mL cylinder, model number SS-4CS-TW-25) that can be isolated from the main vacuum chamber. The method for determination is given in section 2.4. After heating, evolved gas can be swept into the cold traps or vented to the atmosphere using the vacuum pump and associated flow control valve. DESO connections on the cold traps allow for trap removal and counting when full gas removal has been accomplished. For counting, at least two gas exchanges through the system are accomplished followed by system evacuation. Several images of the system are shown in Figure 2, along with annotations indicating important system features.

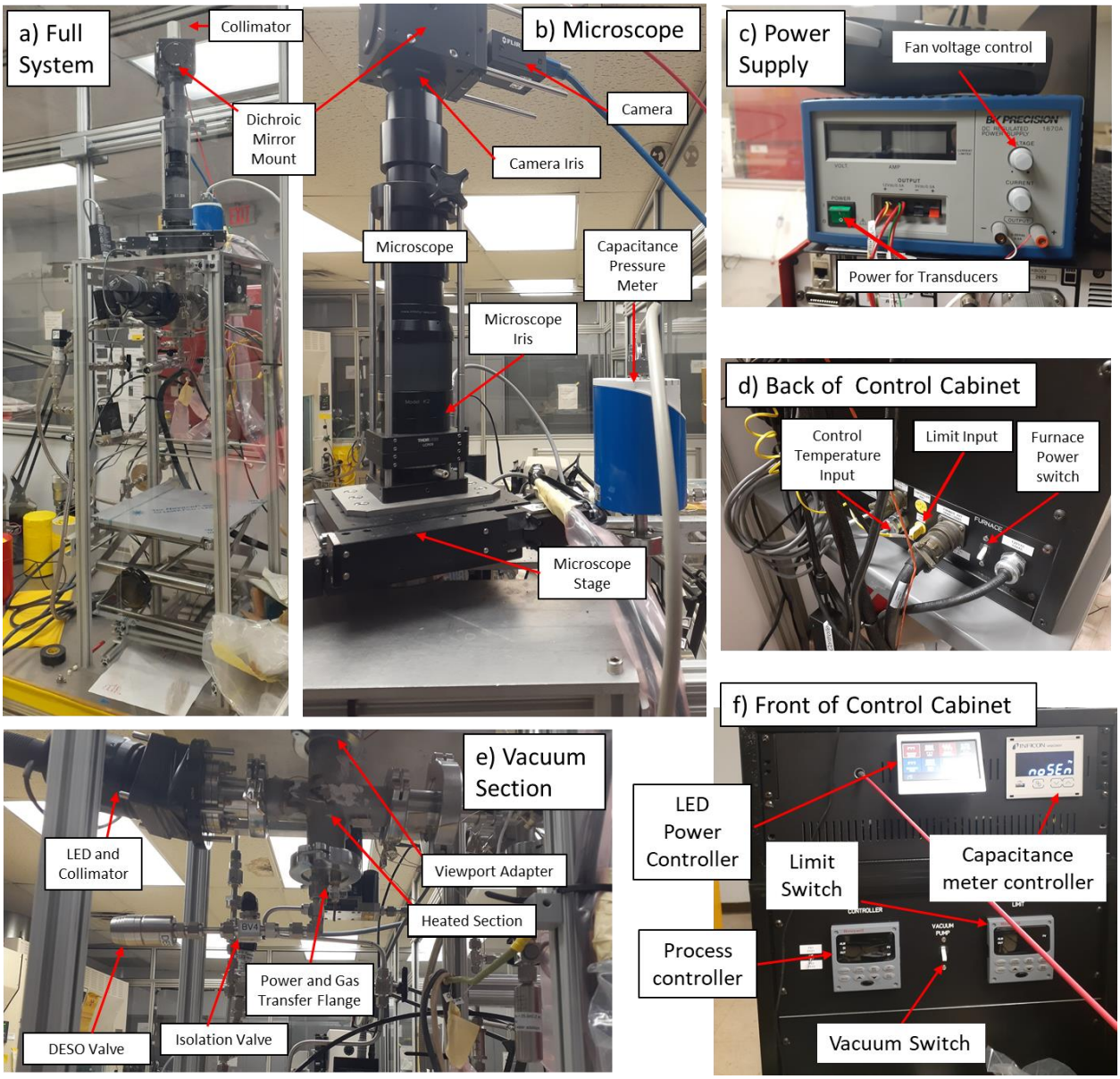

Figure 2. Images of the system and control cabinet. Full testing station, together with major tubing elements (a). Microscope section of the system with important components labeled; capacitance meter shown as it protrudes above the top plate of the frame (b). Power supply used to power the pressure transducers and cooling fans (c). Control cabinet with various components indicated (d and f). Components inside the cabinet — including the serial hub, LabJack, stage motor controller, and spectrometer — are not shown. Test portion of the system's vacuum section, with important features labeled (e).

2.2 CALIBRATION OF THE SPECTROMETER AND TEMPERATURE CALCULATION

Before the temperatures are computed, the spectrometer signal must be calibrated for several reasons. First, the mirrors and gratings within the spectrometer are not perfect and signals must be intensity-corrected for losses within the spectrometer. Second, the optical system is composed of many elements which reduce the amount of light reaching the spectrometer and these must be accounted for in calculating temperatures. A few items, including a fiber optic cable, collimator, microscope, and viewport, should have small losses and above 90-95% transmission rates for most frequencies. However,

some elements strongly affect the signal. These include the dichroic mirror and both irises (see Figure 3). The dichroic mirror transmits well at high frequencies but under 700 nm, the mirror strongly impacts the signal intensity because the nominal cutting wavelength is 650 nm. Iris positions are the most critical because light fractions can be dynamically adjusted from 100% open to fully closed. Thus, calibrations were performed three different camera iris positions, shown as red lines in Figure 3(b), and at 12.5, 25, 50, and 100% open positions for the microscope iris, as determined by the tic marks in Figure 3(a). Red marker indications in Figure 3(b) are between the white arrow and on the iris and the red annotation arrow. Finally, the geometry of the system, absent any losses, affects the light conveyed to the spectrometer. The calibration value at each wavelength is a combination of these effects.

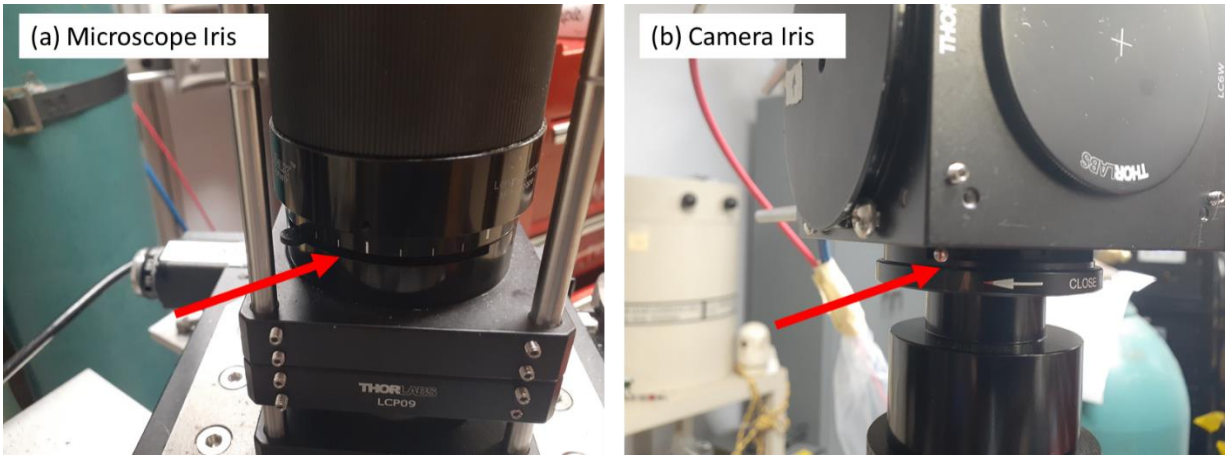

Figure 3. Close-up pictures of the microscope (a) and camera (b) irises.

Temperature is determined from each spectrum by using the well-known Planck's radiation law [9,10],

$$I_{sim}(\lambda) = \epsilon(\lambda)\frac{c_1}{\lambda^5\left[\exp\left(\frac{c_2}{\lambda T}\right)-1\right]}, \tag{1}$$

where, $\epsilon(\lambda)$ is the sample emissivity, c_1 is a constant (=1.19 × 10^{20} W nm^4 m^{-2} sr^{-1}), c_2 is a constant (=1.44 × 10^7 nm K), λ is the wavelength (nm), and T is temperature (K). Observed intensity can then be adjusted by the calibration factor such that at a given temperature,

$$I_{sim}(\lambda) = [I_{data}(\lambda) - I_{back}(\lambda)]\frac{K(\lambda)}{t_{int}}, \tag{2}$$

where, $I_{data}(\lambda)$, $I_{back}(\lambda)$, and $K(\lambda)$ are the observed intensity, background intensity, and system calibration factor, respectively, for the given wavelength, λ. t_{int} is the spectrum integration (collection) time and is used to obtain the proper units (per time) for comparison to the simulated value. Given an accurate temperature and emissivity reading, the calibration factor can be determined as,

$$K(\lambda) = \frac{\epsilon(\lambda)t_{int}}{[I_{data}(\lambda) - I_{back}(\lambda)]}\frac{c_1}{\lambda^5\left[\exp\left(\frac{c_2}{\lambda T}\right)-1\right]} \tag{3}$$

A RCN1350N1 blackbody radiator from HGH USA, Goleta, California with an effective emissivity of >0.99 was used to obtain raw data. The heater cross and associated instrumentation sections were removed, and the blackbody was set up vertically so that the outlet to the blackbody was at the same location as the heater element during a normal test, with a 25 mm aperture (which is the same as the size as the heater).

2.3 SOFTWARE DESCRIPTION

A custom Python code was written to control the instrumentation and collect data. The code consists of three primary Python files specific to this instrument. Three additional python files are included to communicate with the spectrometer and LabJack units through the relevant libraries supplied by the vendors of those units. Additionally, several text files are used to load default test conditions and instrument connections, to establish limits on certain inputs, and to properly configure data channels and the spectrometer.

The code was designed for versatility, allowing for a wide range of experimental conditions and instrument configurations. Although any number of pressure sensors, thermocouples and flow controllers/meters may be connected to the system, there is a limit of 1 of each of the LabJack ADC, the heater system, the camera, and the spectrometer. It is not expected that multiples of any of these units will be required for any test and significant modification to the physical system would be required to accomplish it. Although the system controls much of the experimental flow, it does not have the capability to toggle the LED on/off (the LED power controller is used), turn on/off the vacuum pump (also a manual switch), adjust any of the valves (all of which are manual, except for the flow controllers) or move the stage (this is done with a stand-alone program from the stage vendor). Other elements, including spectrum acquisition, temperature and pressure monitoring, system alerts, safety shutdowns, image collection/saving, heater setpoint and power control, and data presentation are handled by the program.

The program is built primarily around Python's Tkinter graphical user interfaces (GUIs) (an exception is the camera-control GUI). On startup, an infinite loop is created which builds the data entry screen (see Figure 4). Colored boxes group entries according to category. While all elements of the primary GUI are not discussed in this work, a few notes are valuable. First, most changes to this screen from one test to another will occur only in the black box on the top left of the screen where the experiment file location, experiment name and temperature programming are listed. An unlimited number of temperature set points can be programmed, with either universal hold time and ramp rate or unique ramp rate and hold time for each point. The remainder of the entries relate to instrument connections (the right side of the screen) or changes in the spectrometer settings, calibration file (and format) used, and settings of the runtime GUI.

Once the requested inputs have been provided, the system checks for input consistency and reports back any errors. Certain errors (such as no flow controllers/meters being listed) will generate a simple warning stating the consequence (no gas flow control is possible without controllers/meters in the program). Other errors, such as improperly specifying connections, or failing to provide a ramp rate for a given set point will lead to "Fatal Error" notifications. Such errors make it impossible for the system to execute a test, so the program will not proceed until they are corrected.

When fatal errors are corrected, the inputs can be accepted, and the input GUI will close. A second GUI, Figure 5, opens and populates all graphs and data entry locations. Graphs are seeded empty, and all data entry locations display a "waiting" notification. On "Start" activation, the system starts the experiment control function. The experiment control function is largely an administrator, which delegates the work of the code to three separate parallel processes controlling the camera, spectrometer, and other data and control operations, respectively. A fourth process is created to handle display of notification logs. Each of

these is required to facilitate rapid display of the data and minimize instrumentation lags, particularly for the camera.

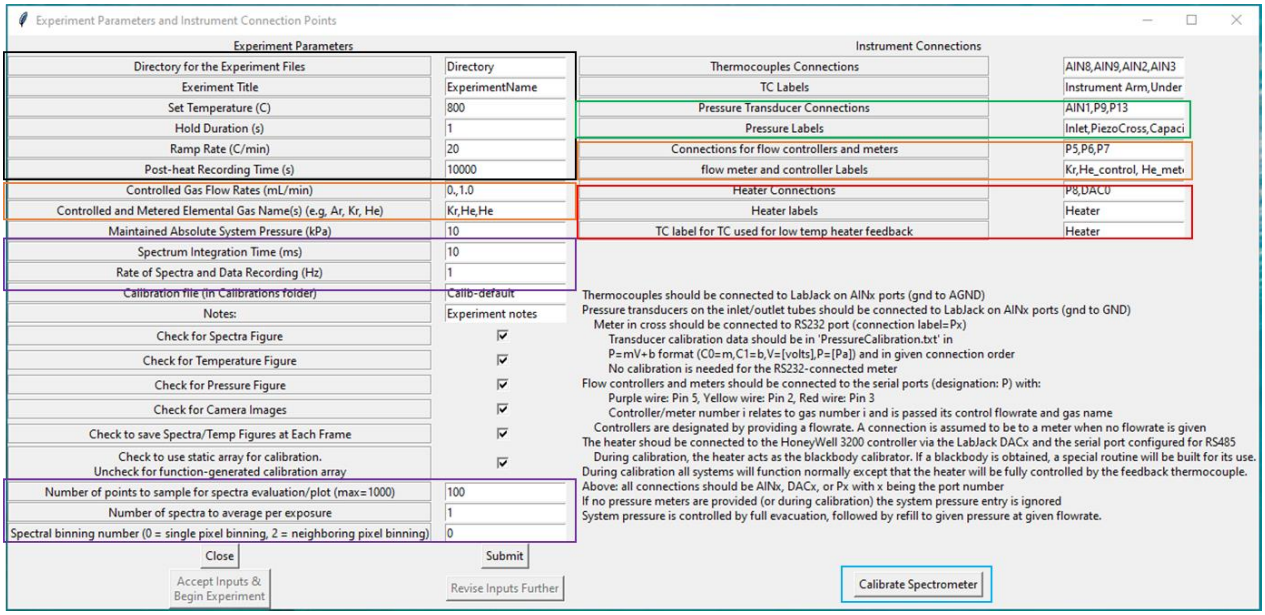

Figure 4. Input selection screen of Fuel Visualization System software. Overlaid boxes are referenced in the text.

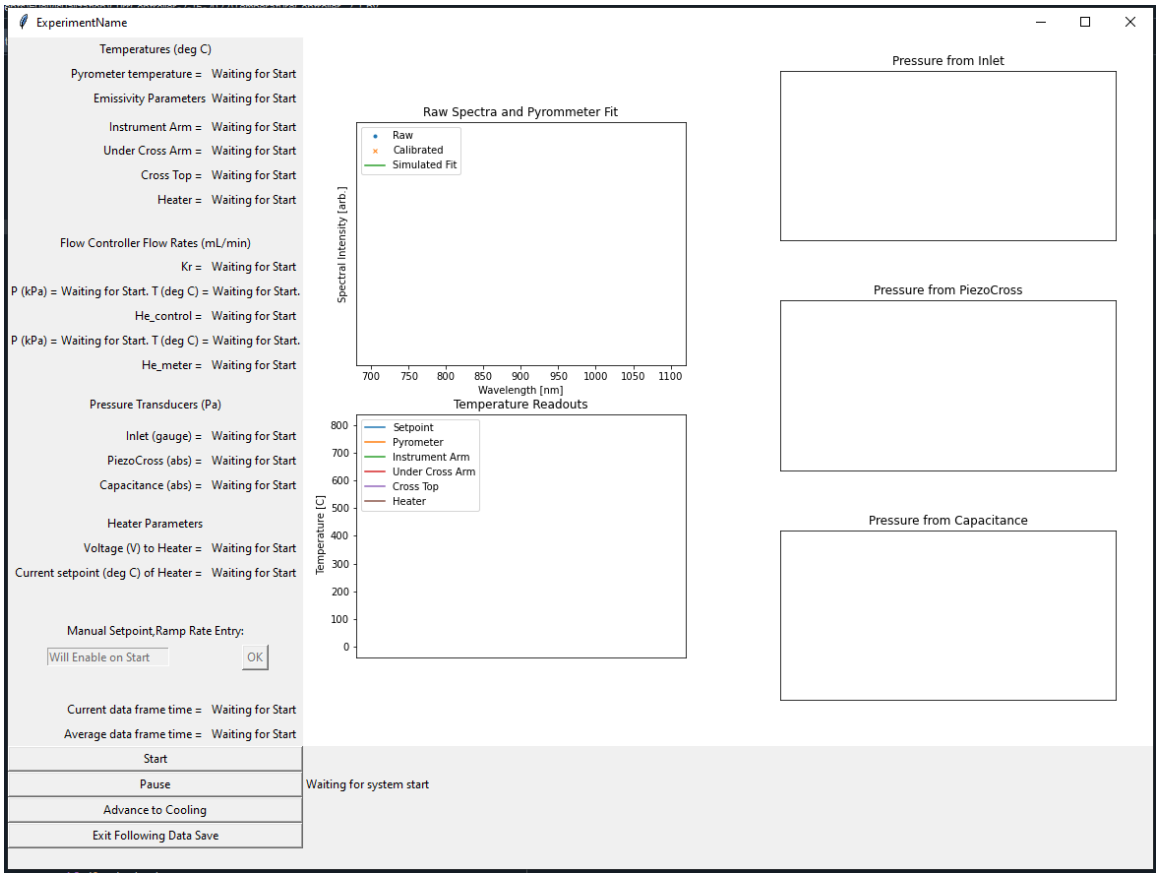

Figure 5. Experiment management GUI prior to system start.

Each processor is built with its own data pipe with one end in the parent process and one end in the new process. This pipe is used primarily to pass status messages between the processors. If at any point the spectrometer or data processor fails, then the administrator uses these pipes to request shutdown in all processes. Otherwise, the content of the lists passed in these pipes is used to request another data stream or indicate instrument status. In addition to the pipes, the spectrometer and notification display processes also use a data queue to pass larger data sets. For the spectrometer, the data passed across consists of the spectral outputs. Notification strings are passed across the notification queue, which is continuously checked by the notification processor.

When the camera processor is started it builds a PyQt GUI that allows the camera to start and stop at any point. On start, the camera is turned on and attempts to continuously collect and save images at a rate of up to 5 Hz. Typically, 3 Hz is achieved. Collected images are saved and then displayed at a default of 800 × 800 pixels, a value that can be dynamically adjusted in the GUI. Similarly, the notification process creates a GUI continuously checks for new data on its queue and then displays that information. Both processors send and receive READY and STOP signals to and from the administrator, but otherwise they proceed at their rate.

However, the data management and spectrometer processors, do not create GUIs or run at their own pace. On initialization, the spectrometer process checks for communication with the instrument and prepares it to collect data. It then waits for a READY signal to collect a spectrum, analyze it, return the relevant data to the administrator, and save the files. The data manager has significantly more operations to performs on startup. It is responsible for managing communication with the PID controller, LabJack, pressure units and flow units. During setup, system notices are continuously transmitted, especially because some, like flow meter zeroing, may require operator action. After setup, the data manager also waits for a READY signal to proceed.

Once everything is prepared, the administrator enters its own infinite loop which only exists when the test is complete through normal end or error. At the start of this process, the test is in the evacuation-and-refill stage. A checkbox appears on the bottom of the run time GUI, Figure 5. When activated, the system proceeds through each step, providing relevant notifications. After the final refill, the user checks the box again to begin heating the sample. Throughout this process, all four daughter processes run and provide data displayed by the program and saved in a text file. Once heating begins, the administrator function calculates the proper setpoint based on time of operation and requested set point, ramp rate, and hold time lists. The set point is then sent to the data manager which conveys it to the PID controller along with the current system temperature. If at any time the system is ended or crashes, then the set point automatically returns to room temperature.

Once the final temperature has been held for the requested time the system the set point is adjusted to room temperature, and data are collected until the test is ended. On test end, STOP signals are sent to all processors, a compiled data file is saved, and the only option left on the run time GUI is to close the system. Closing the GUI leads to the test GUI being re-opened automatically to perform another test. This can be closed out if a follow-up test is not desired.

2.4 SYSTEM VOLUME DETERMINATION

A nominally 25 mL sample cylinder was added to the system cross to determine chamber volume. Prior to this addition, the sample cylinder volume was evaluated four times with water additions using graduated cylinders calibrated to-deliver. The sample cylinder was completely filled, and the added water volume was recorded. All water was emptied, and the cylinder was thoroughly rinsed with acetone to remove residual water droplets and allowed to air out for at least 5 min. Using this method, the sample cylinder volume was determined to be 25.6 ± 0.2 ml. After volume recording, the sample cylinder was

connected to a ball valve, with internal volume within the error of the chamber measurement, based on dimensional analysis. This valve was then connected to the system via one of the KF16 ports.

The volume of the test chamber was then determined by evacuating the entire test chamber to about $P_b \approx$ 1100 Pa, while the sample cylinder's isolation valve was open. This ensured that both the test chamber and sample cylinder have an absolute pressure of P_b. The isolation valve was then closed and the test chamber was evacuated to $P_e \approx 45$ Pa. The isolation valve was then opened, allowing the pressure between the sample cylinder and test chamber to equalize to a refill pressure, P_r. The background pressure of 1100 Pa was chosen because it is near the upper limit of the capacitance meter (1325 Pa), which is more sensitive than the transducer, thus allowing measurements of the test chamber volume, one with each meter. This process was performed three times. Test chamber volume was then calculated using the ideal gas law,

$$V_{test} = V_{sample}\left(\frac{P_b - P_e}{P_r - P_e} - 1\right), \tag{4}$$

and the propagated error is found by

$$\sigma_{V_{test}} = \sqrt{\left[\sigma_{V_{sample}}\left(\frac{P_b - P_e}{P_r - P_e} - 1\right)\right]^2 + \left(\frac{\sigma_{P_r} V_{test}}{P_r - P_e}\right)^2 + \left(\frac{\sigma_{P_b} V_{sample}}{P_r - P_e}\right)^2 + \left[\frac{\sigma_{P_e} V_{sample}(P_b - P_r)}{(P_r - P_e)^2}\right]^2}. \tag{5}$$

The computed chamber pressure is reported in

Table 2. Both the capacitance meter and pressure transducer yield similar chamber volumes at approximately 560 mL with 3 mL of error. If the error by propagation is used (**5**), instead of standard deviation then the error increases to about 5 mL and 10 mL for calculations using the capacitance meter and transducer, respectively. Propagated error is a more conservative estimate of error that takes account of every source of error and compounds all errors, whereas statistical error is usually more representative of actual data when several observations are available. Relying only on statistical error in data, the computed chamber volume from each source is just within 1σ error. However, the increased error from propagation results in statistical similarity between both measurements, within 1σ error.

Table 2. Test chamber computed using data from three volume measurements. Measurements were computed using (4). Statistical error is the standard deviation across the three tests.

Method	Volume (mL)	Statistical error (mL)
Capacitance	561	3
Transducer	566	3

For this report, the statistical error is expected to be more accurate because the capacitance meter has better low-pressure resolution than the transducer. This is the reason that propagated error yields a much higher error (10 mL) for the transducer than for the capacitance meter (5 mL). Using the capacitance meter as the primary gas-release monitor, the number of moles of gas released and approximate error should be as follows:

$$n_{release} = \frac{P_{meas} V_{test}}{RT} \tag{6}$$

$$\sigma_{n_{release}} = \sqrt{\left(\sigma_{P_{meas}} \frac{V_{test}}{RT}\right)^2 + \left(\sigma_{V_{test}} \frac{P_{meas} V_{test}}{RT}\right)^2 + \left(\frac{\sigma_T n_{release}}{T}\right)^2} \quad (7)$$

where T is the absolute temperature, R is the universal gas constant, P_{meas} is the measured pressure increase during the test, and V_{test} is the volume of the chamber reported in

Table 2. During the test, the number of released moles is difficult to evaluate because most of the chamber is under 100 ℃, but the sample itself, along with released gases and gases coming in contact with the sample, can be near 800 ℃. This means that the third term in (7) becomes large since the effective temperature of the gas in the system is unknown at any time. Thus, the released gas is best calculated only when σ_T is low (i.e., when the system temperature is near to room temperature). When calculating released gas at room temperature $\sigma_T \approx 1$ K, T = 294 K, $\sigma_{V_{test}}$ = 3 Pa, and R = 8.3145x10^6 Pa-mL/K-mol, (7) becomes

$$n_{release} \approx 2.296x10^{-7} P_{meas} \quad (8)$$

$$\sigma_{n_{release}} \approx \sqrt{5.272x10^{-14}\sigma_{P_{meas}}^2 + 2.116x10^{-18}P_{meas}^2}. \quad (9)$$

The approximations shown in (**8**) and (**9**), are fairly sensitive to the σ_T value and 1 K is reasonable for cooling times > 1 hour. When the data are taken after much smaller cooling times (<15 min), the temperature error can be as high as 5 ℃ and the original equations must be used. The value of $\sigma_{V_{test}}$ only weakly affects the error calculation; and there is about a 5% increase in error if 5 Pa is used for $\sigma_{V_{test}}$ instead of 3 Pa.

2.5 STAND-UP TESTS WITH HYROGEN-INFUSED TITANIUM FOILS

Titanium foil (99.99% pure) was purchased from Sigma Aldrich, St. Louis, Missouri and cut into small pieces for hydriding. Foils were gas-charged with hydrogen using a custom system that precisely controls hydrogen flow rate, hydrogen partial pressure, and temperature. This system was previously reported by Hu et al [11]. The hydriding procedure was initially determined using pressure-composition-temperature equilibriums from the Ti/H binary system [12]. Foils were cleaned in acetone in an ultrasonic bath before being inserted into the retort. During processing, after undergoing argon and hydrogen purge at room temperature, the system was heated to 600 ℃ at 10 ℃/min under high vacuum (<10^{-4} Pa) and held for 6 hr, and then it was cooled to 550 ℃ at 20 ℃/min and held at that temperature for 1.5 hours still under high vacuum. After the 1.5 hr hold, the furnace was kept at 550 ℃, and H_2 was introduced at 15 sccm until the pressure reached 400 Pa. The sample was then held at 550 ℃ and 400 Pa under 5 sccm flow of H_2 for 15 hr. The system was then cooled to 200 ℃ at 2.5 ℃/min under 5 sccm of H_2 flow at 400 Pa, and then the sample was allowed to cool naturally under vacuum until it reached room temperature. This procedure was adopted similar to Hu et al [11] with adaptations for the TiH_x system. Normally, the pressure would be determined as a function of temperature during cooling to hold the composition constant, but that was not performed in this study because there was no precise hydrogen target.

The foil segment reported in this work initially had an as-cut mass of 233.9 ± 0.1 mg. After hydrogen treatment, the sample mass increased to 241.9 ± 0.1 mg and became brittle. Assuming all of the mass was added as dissolved hydrogen, approximately 4 mmol H_2 was added to the system. The sample was further cut to 12.0 mg, corresponding to 0.2 mmol H_2. Based on the chamber volume of 561 mL from section 2.4, if all the estimated gas were released, then the chamber pressure would increase by about 930 Pa, which is within the range of the low-pressure capacitance meter.

After preparation, two tests were performed. The first was a “blank test” to evaluate gas emissions by the system (which includes the heater assembly and the AlN sample plate) in the absence of a sample. In the second test, the actual hydrogen release was measured by adding the 12.0 mg TiH_x sample was to the sample plate. Heating was accomplished at 20 ℃/min to 800 ℃, followed by immediate cooling.

3. RESULTS OF SYSTEM CALIBRATION AND STANDUP TESTING

3.1 RESULTS OF SYSTEM CALIBRATION USING THE BLACKBODY RADIATOR

Calibration was performed using spectra at 800 °C with 12 iris configurations with the blackbody radiator in place of a heated sample. Each calibration scan was performed using 20 ms integration times and 100 averages to minimize electronic noise. The configuration used in these tests (25% open microscope aperture and partial close [unquantified] of the pre-mirror aperture) is reported in this work. Other configurations showed similar results. Between iris configurations, the calibration factors only changed in magnitude, due to variation in the amount of light reaching the spectrometer. Figure 6(a) presents the 800 °C calibration curve (purple) on the second y-axis. The first y-axis shows the spectral intensity values of the background (green), 600 °C (yellow), 700 °C (orange), and 800 °C (blue) calibration scans. Figure 6(b) shows the calibrated spectral intensities at the same temperature conditions. Dashed curves in Figure 6(b) represent simulated data from (**1**) at a given temperature, and individual points, which appear as lines because of density, represent the calibrated experimental data: that is, (**2**) was applied to the data in Figure 6a.

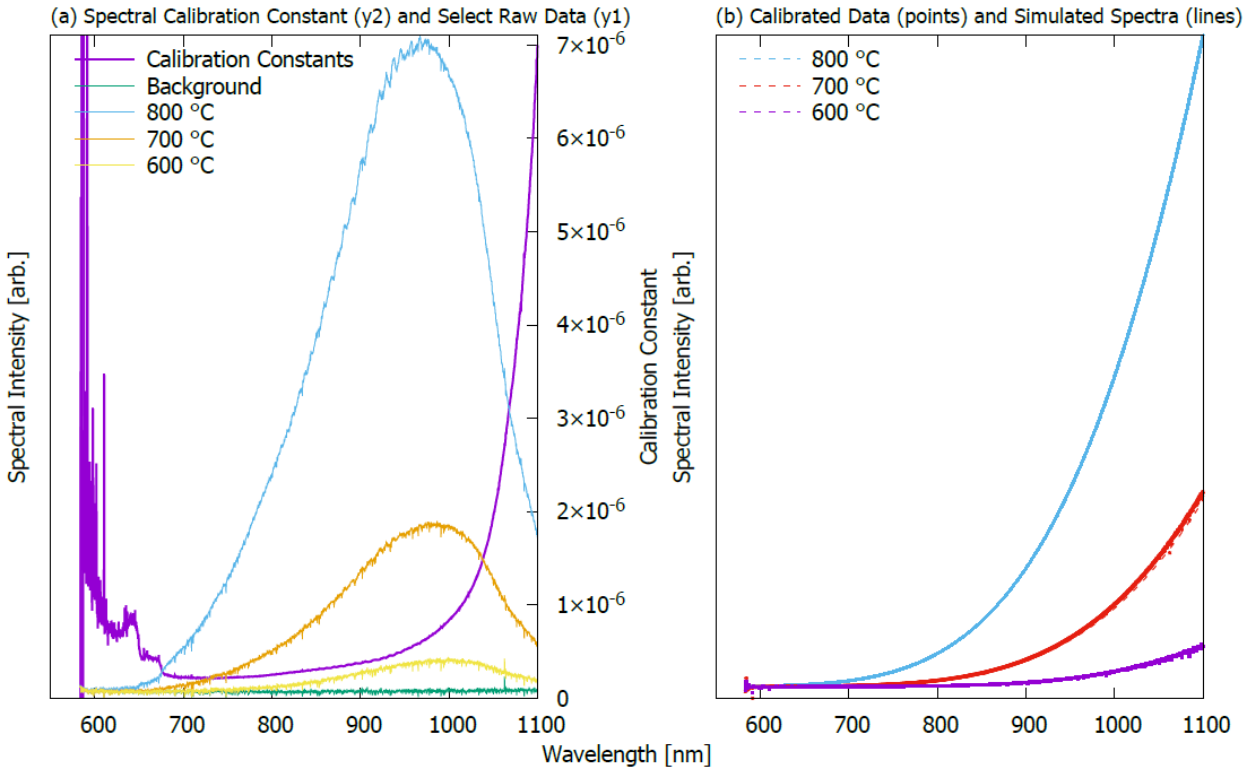

Figure 6. Results of spectrometer calibration with blackbody unit. Raw spectral intensity (left y-axis) reported by the spectrometer in the background, and at 600, 700, and 800 °C, listed in order of intensity and as shown in the legend. The right y-axis shows the calibration curve calculated at 800 °C (a). Calibrated spectral data (points) and corresponding simulated data (dashed lines) (b). Calibration was conducted at 800 °C so there is perfect overlap between the calibrated data curve and the simulated curve. At lower temperatures, the calibrated and simulated data sets are distinguishable.

Several important features about the calibration in these data should be noted. In Figure 6(a), the purple (calibration) curve is fairly smooth and continuous as a function of wavelength, except at low (<700 nm) wavelength. At low wavelength, the calibration curve is discontinuous and contains several steps. Moreover, the curve is overall inversely proportional to wavelength, rather than directly proportional, as

at higher wavelength. This low-wavelength anomaly is caused by the dichroic mirror, which has a cutting wavelength of 650 nm. As the wavelength decreases, more light is lost to reflection so the calibration constant increases to compensate for the loss. The effect of the mirror is also apparent in the raw data and is most clear in the spectral data from 800 °C (the blue curve in Figure 6a), where the raw data show significant intensity drops corresponding to large increases in the calibration value. As a consequence, the pyrometry calculations only use wavelengths from 700 to 1100 nm.

Finally, Figure 6(a) implies an ideal form of the calibration curve. Again, particularly noting the blue curve in Figure 6(a) (800 °C), the raw data near the peak intensity values at around 900 – 1000 nm are somewhat sinusoidal or jagged. This effect is not related to noise in any particular scan, because 100 averages were taken for each spectrum. Additionally, every scan with significant spectral intensity showed similar jaggedness at the same wavelength values. Although this is not clearly visible in Figure 6(a), it is also apparent that each pixel has its own, distinct calibration value, likely stemming from mirror and grating imperfections within the spectrometer. These local spectral features must be accounted for to obtain accurate temperature compositions. Thus, the calibration curve for this work consisted of the entire calibration array, rather than a polynomial, or other smoothed function, fit to the calibration curve.

As confirmation that the 800 °C calibration values are reasonable, the calibration was applied, using (**2**) to the other temperature data sets in this work, and the 700 °C and 600 °C data sets are shown with the 800 °C data set in Figure 6(b). At 800 °C, the spectral data perfectly calibrates the spectrum to agree with the simulated spectrum. This is because the calibration curve is not smoothed at all by a fitting function and application of (**2**) is just the reverse of calculating a calibration curve in the first place. At lower temperatures, however, the dashed lines and points are distinguishable, but only slightly, indicating a calibration that is usable for somewhat lower temperatures as well. However, temperatures under 400–500 °C cannot be determined by pyrometry with the current setup because of signals that are almost entirely below background. Improvement of the temperature resolution is reserved for future work.

3.2 GAS EVOLUTION DEMONSTRATION TEST

The gas evolution demonstration test with the TiH_x foil was performed at a 20 °C/min ramp rate to 760 °C. The original test target temperature was 800 °C, which was not achieved because of an incorrect reading from the pyrometer that led to an early transition to cooling. Because the test was within 40 °C of the target temperature, the system was allowed to finish cooling. During the test, the pyrometer could not be used because of significant shielding of the hot surface by alumina beads on the thermocouple wires, as shown in Figure 7. Optical shielding of the sample was unavoidable in this test due to a need to replace the heating element just before the test. The new heating element was not perfectly level, and it was not possible to position the sample properly. Design changes are planned in the heater substrate geometry to mitigate this problem for future tests.

Figure 7 shows optical images of the sample region at the beginning of the heating portion of the test (a), and at 400 (b), 500 (c), 600 (d), 700 (e), and 760 °C (f). For the first few hundred degrees, the sample appeared to be unchanged. However, above 500 °C, the sample began to shift somewhat, as shown in Figure 7(d – f). This is likely due to the heating element softening at higher temperatures and causing the sample plate to slightly adjust its position. Throughout the test, no change in the appearance of the foil was observed apart from the expected red-light emission at high temperatures (see Figure 7f).

Because the thermocouple wire was placed directly on the AlN disk surface, its temperature was used as a stand-in for the pyrometry data. Temperature and pressure readouts are presented in Figure 8. The thermocouple data in Figure 8 are displayed as an orange curve with values corresponding to the primary y-axis (left). Pressure data are shown by the blue curves on the secondary (right) y-axis. Both the transducer (solid curve) and capacitance meter (dashed curve) are shown in Figure 8. For most of the test,

both meters agree on the pressure, within a few percent. Around 55 min, the capacitance meter reached its maximum read value, whereas the transducer continued to display the correct pressure value.

Figure 8 also shows the difference in pressure resolution between the transducer and the capacitance meter. Especially at higher pressures, the resolution significantly degraded on the transducer, and pressure was less well resolved compared to the capacitance meter. This finding bolsters the discussion in Section 2.4 regarding the preferential use of the capacitance meter to determine system volume.

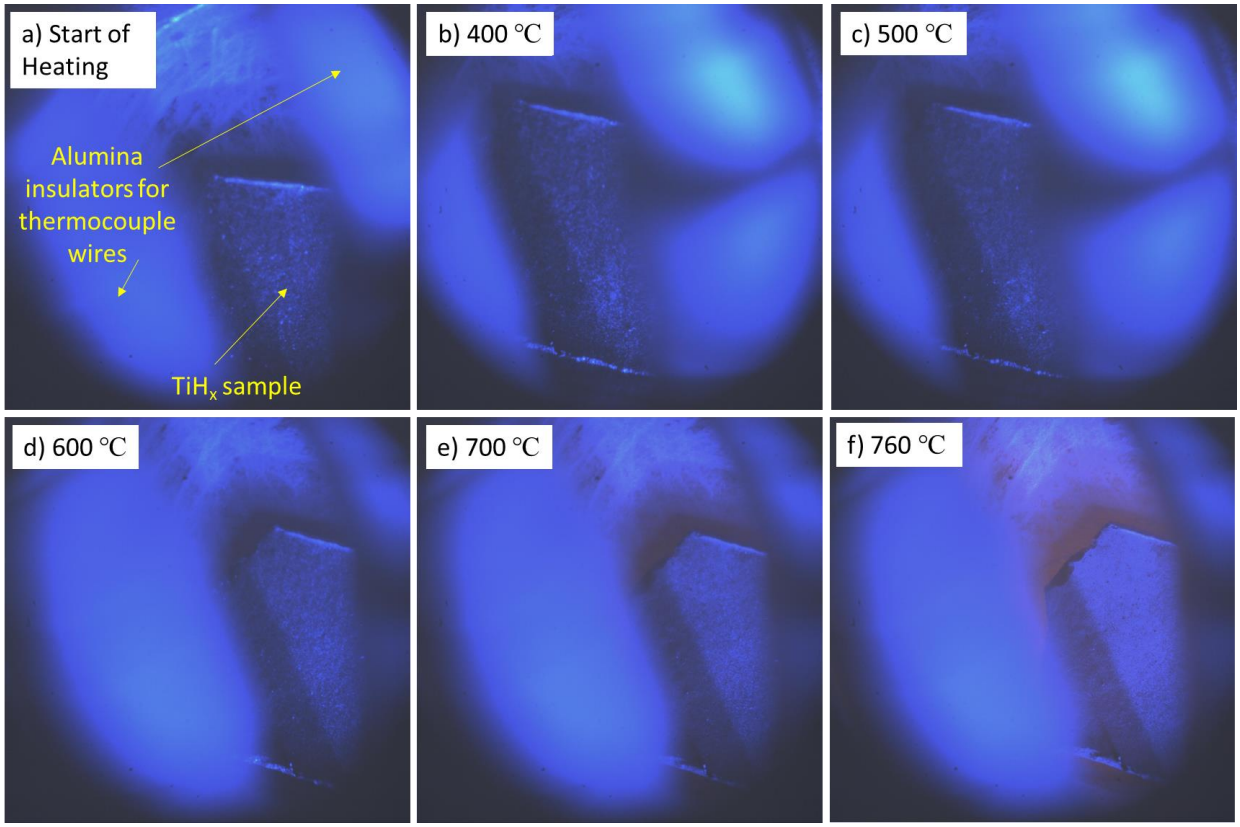

Figure 7. Optical images of the heated TiH_x sample at various stages in the test. Images are shown at (a) the start of heating, and at sample temperatures of (b) 400 °C, (c) 500 °C, (d) 600 °C, (e) 700 °C, and (f) 760 °C. Annotations in (a) indicate the foil location, as well as the alumina insulators for the thermocouple wires. The AlN sample plate is holding the TiH_x sample and is the only other feature in the images.

As expected from the discussion in section 2.4, the system pressure was significantly higher when the sample was hot than after it cooled. Additionally, by examining the pressure curve at low temperatures, a leak rate into the system of about 0.022 Pa/s was inferred. This leak rate is attributed to seal imperfections and represents approximately 5 nmol/s of gas ingress at room temperature. In the sample-free test, approximately 32 µmol of gas was released by system components. These artifacts can be accounted for by estimating the amount of gas in the system at the end of the test, per (6 and subtracting off the system-released gases and gases added by ingress through small leaks. Accordingly, the TiH_x foil is estimated to have released 0.18 mmol of H_2, which is only slightly less than the 0.21 mmol H_2 originally estimated to be in the sample.

Moreover, gas was not released from the hydrogen-containing titanium until approximately 35 min into the test, when the temperature reached about 450 °C. Gas release increased quickly with temperature until approximately 43 min, when the temperature reached a maximum value of approximately 580 °C, and gas

release became mostly linear with temperature. These observations are consistent with literature observations of TiH_x decomposition [13].

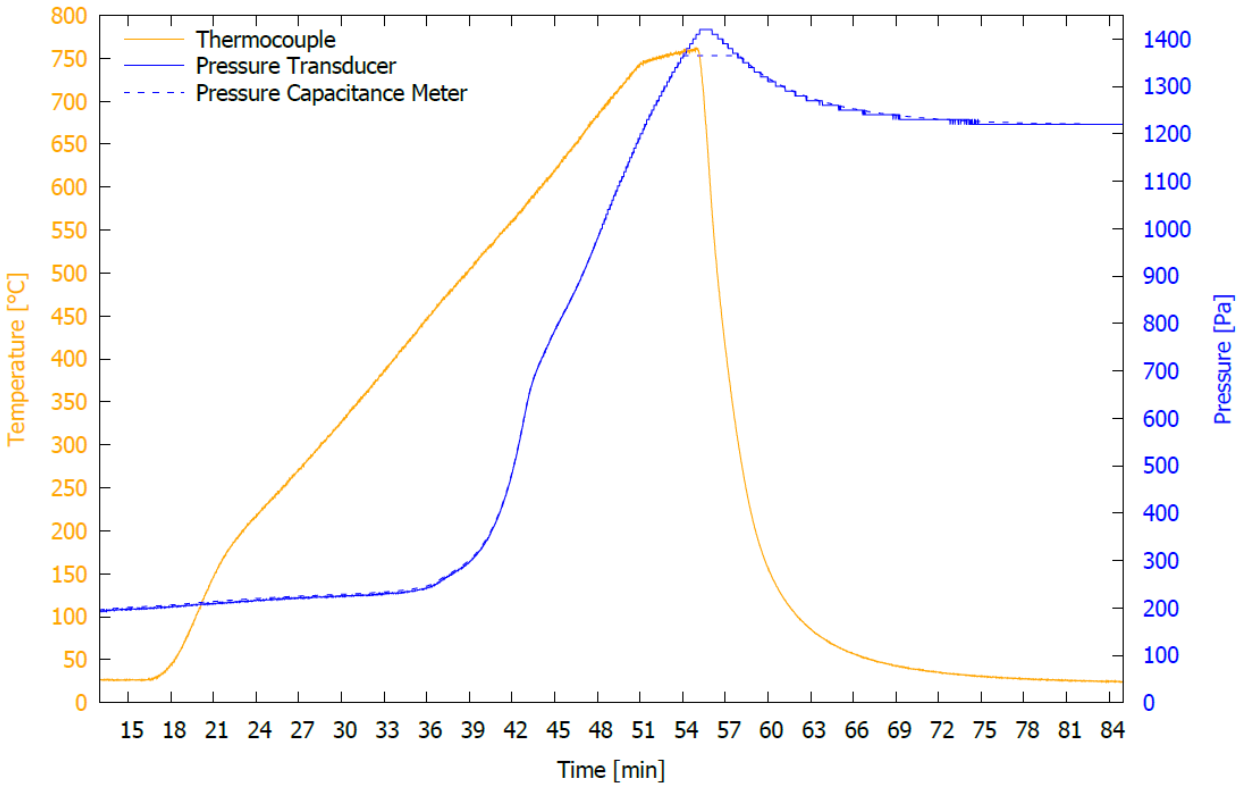

Figure 8. Pressure and temperature data as a function of testing time. Only the testing portion starting just before sample loading is shown. The y-axis shows temperature (orange) as read by the thermocouple, and the secondary y-axis shows pressure. Pressure is recorded both by the transducer (solid line) and the capacitance meter (dashed line).

4. CONCLUSIONS AND FUTURE WORK

A system was designed and built to evolve and observe fission gases emitted during loss-of-coolant (LOCA)-type events. Fuel is heated in an evacuated environment and conditions can be observed with a camera, spectrometer, a thermocouple, and two pressure gauges. The system is primarily run and monitored with a customized Python routine which manages the heater controls, gas flow, and data collection and analysis. In this report, the system capabilities are described and the system is showcased using a TiH_x foil to evolve H_2 gas over a temperature range similar to that expected for gas evolution during transients with high burnup fuel.

Future work will be aimed at improving the system's capabilities. Whereas some work will address general code robustness and usability, the primary focus of these improvements will be in the pyrometer to improve the sample selection (i.e., eliminate view of the sample holder while maintaining sufficient spectrometer signal). Additionally, there are improvements planned in the pyrometer solver to improve the accuracy of data fits and provide versatility for dynamic changes in the solver parameters at/during runtime. Beyond these items, first-use of fuel samples with collection and measurement of radioactive gas is planned and results from that test will be used to iterate the instrument design.

5. ACKNOWLEDGMENTS

The authors gratefully acknowledge the helpful insights on Yong Yan, and Chris Petrie. Tyson Jordan, Zachary Burns, and Scott Thurman also provided helpful assistance in the building and operation of the instrument. Thanks also to Rachel Seibert for her helpful technical comments and to Rose Raney for her helpful technical edits on the manuscript.

6. REFERENCES

[1] C. Le Gall, S. Reboul, L. Fayette, T. Blay, I. Zacharie-Aubrun, I. Félines, K. Hanifi, I. Roure, P. Bienvenu, F. Audubert, Y. Pontillon, J.L. Hazemann, "MOX fuel Microstructural Evolution during the VERDON-3 and 4 Tests," *J. Nucl. Mater.* 531 (2020). https://doi.org/10.1016/j.jnucmat.2020.152015.

[2] T. Vidal, L. Gallais, R. Burla, F. Martin, H. Capdevila, S. Clément, Y. Pontillon, "Optical System for Real-Time Monitoring of Nuclear Fuel Pellets at High Temperature," *Elsevier* (2020). https://doi.org/10.1016/j.nucengdes.2019.110383.

[3] Y. Pontillon, M.P. Ferroud-Plattet, D. Parrat, S. Ravel, G. Ducros, C. Struzik, I. Aubrun, G. Eminet, J. Lamontagne, J. Noirot, A. Harrer, "Experimental and Theoretical Investigation of Fission Gas Release from UO_2 up to 70 GWd/t under Simulated LOCA Type Conditions: The GASPARD Program," in: *Proc. 2004 Int. Meet. LWR Fuel Perform.* {2004) 1025.

[4] M.S. Veshchunov, V.E. Shestak, "Modelling of Fission Gas Release from Irradiated UO_2 Fuel under High-Temperature Annealing Conditions," *J. Nucl. Mater.* 430 (2012) 82–89. https://doi.org/https://doi.org/10.1016/j.jnucmat.2012.06.048.

[5] L.O. Jernkvist, "A Review of Analytical Criteria for Fission Gas Induced Fragmentation of Oxide Fuel in Accident Conditions," *Prog. Nucl. Energy.* 119 (2020) 103188. https://doi.org/https://doi.org/10.1016/j.pnucene.2019.103188.

[6] M. Tonks, D. Andersson, R. Devanathan, R. Dubourg, A. El-Azab, M. Freyss, F. Iglesias, K. Kulacsy, G. Pastore, S.R. Phillpot, M. Welland, "Unit Mechanisms of Fission Gas Release: Current Understanding and Future Needs," *J. Nucl. Mater.* 504 (2018) 300–317. https://doi.org/https://doi.org/10.1016/j.jnucmat.2018.03.016.

[7] Bales, M., A. Chung, J. Corson, L. Kyriazidis, *Interpretation of Research on Fuel Fragmentation , Relocation, and Dispersal at High Burnup* US Nuclear Regulatory Commission, RIL 2021-13 (2021).

[8] J.R. Rumble, ed., *CRC Handbook of Chemistry and Physics*, 102nd ed., CRC Press/Taylor & Francis, Boca Raton, FL, n.d.

[9] A. Araújo, R. Silva, "Surface Temperature Estimation in Determined Multi-Wavelength Pyrometry Systems," *Rev. Sci. Instrum.* 91 (2020) 54901. https://doi.org/10.1063/5.0005676.

[10] D.P. DeWitt, G.D. Nutter, eds., *Theory and Practice of Radiation Thermometry*, John Wiley & Sons, Inc. (1988).

[11] X. Hu, D. Schappel, C.M. Silva, K.A. Terrani, "Fabrication of Yttrium Hydride for High-Temperature Moderator Application," *J. Nucl. Mater.* 539 (2020) 152335. https://doi.org/https://doi.org/10.1016/j.jnucmat.2020.152335.

[12] A.D. McQuillan, "An Experimental and Thermodynamic Investigation of the Hydrogen-Titanium System," *Proc. R. Soc. Lond. A. Math. Phys. Sci.* 204 (1950) 309–323. http://www.jstor.org/stable/98686.

[13] H. Liu, P. He, J.C. Feng, J. Cao, "Kinetic Study on Nonisothermal Dehydrogenation of TiH_2 Powders," *Int. J. Hydrogen Energy*. 34 (2009) 3018–3025. https://doi.org/https://doi.org/10.1016/j.ijhydene.2009.01.095.